Study on Cavitation Characteristics of Rotating-Sleeve Flow Distribution System

R. Liu[1], T. Zhang [1], S. Du [2†], Q. Zhao [1†] and H. Zhang [2]

[1] *Power Integration and Energy Storage Systems Engineering Technology Center, Qingdao University, Qingdao 266071, China*
[2] *School of Electromechanical Engineering, Qingdao University, Qingdao 266071, China*

†*Corresponding Author Email: 2018025250@qdu.edu.cn*

ABSTRACT

As Rotating-sleeve Flow Distribution System (RFDS) running, the cavitation of the hydraulic pump may lead to the decreased volume efficiency, increment of vibration and noise, then affecting the operation of system. To deeply analyze the cavitation characteristics of RFDS, the Singhal cavitation model of RFDS was established, meanwhile corresponding experiments were carried out. Cavitation characteristics of RFDS were investigated under various revolving speed, inlet pressure and CAM groove profile. The results demonstrate that the variation trend of experimental volumetric efficiency is the same as that of simulation results. The maximum error is 2% and 3.2% at different rotating speeds and different inlet pressures respectively. Maximum gas volume fraction and cavitation time ratio increase monotonically as the rotating speed increases, and volumetric efficiency increases first and then decreases with the increase of rotating speed. Volumetric efficiency reaches up to 92.13% under the rotating speed of 500r/min. The increased inlet pressure can slow down the cavitation of RFDS and improve volumetric efficiency. Linear profile exhibits the best cavitation characteristic under both different rotating speed and inlet pressure.

1. INTRODUCTION

The hydraulic pump is the power device of hydraulic system, the plunger pump has the advantages of a positive displacement pump with high efficiency, high pressure, large flow and so on, which is widely used in vehicles, ships, aviation and other fields with large power transmission demand (Zhang *et al*. 2007; Mikalsen *et al*. 2007). The plunger pump usually uses a one-way valve or solenoid valve for flow distribution. Due to the lag of the check valve, especially in the high speed reciprocating movement of the plunger with serious lag, resulting in poor self-priming ability, increased leakage, large local throttling pressure loss, volume efficiency loss; Solenoid valve needs special measurement and control device to ensure the valve and plunger motion in tune, which increases the complexity of the structure and manufacturing cost; In addition, the valve and the external pipe joint make the pump body large, difficult to install and arrange, and increase the working noise (Lao *et al*. 2015).

As a new type of plunger pump, RFDS uses the reciprocating motion of the plunger to drive the one-way rotation of the sleeve to realize the distribution function, which has many advantages including small volume, low cost, high volume efficiency and stable performance (Zhang *et al*. 2015). At the initial stage of oil absorption, there is a large negative pressure in the system. Air or oil vapor is separated from the oil and two phases coexist, resulting in cavitation (Zhang, 2004; Wylie *et al*. 1978). Cavitation will reduce the volume efficiency of the system, resulting in strong vibration and noise (Murovec *et al*. 2020; Richard *et al*. 2002), and seriously influencing RFDS.

The traditional cavitation analysis method has been developed, but there are some limitations in engineering application. At the beginning of this century, CFD cavitation models developed rapidly, among which the three models proposed by respective Schnerr *et al*. (2001), Singhal *et al*. (2002), and Zwart *et al*. (2004) were the most typical ones, which attracted extensive attention. Huang *et al*. (2009) wrote relevant control programs embedding Kubota, Singhal, Merkle and Kunz models in the simulation calculation, achieving cavitation flow patterns around Clark-y hydrofoil, which were comparable to the experimental

results, it was observed that Singhal model was the most comprehensive. Gao et al. (2018) analyzed the distribution of gas phase volume fraction under different positions of the hydraulic plunger pump's plunger cavity through numerical simulation, which found that cavitation mainly occurred in the unloading groove of the plunger cavity and distribution plate in the suction area, it could be decreased by reducing the inclination angle of the inclined plate, increasing the depth of the unloading groove. Yuan *et al.* (2015) proposed a dynamic fluid model for the cavitation phenomenon, which may occur during the working process of axial piston pump, the internal mechanism of gas influencing pump characteristics was analyzed. Liu *et al.* (2015) conducted numerical simulation of cavitation flow of swashplate axial piston pump based on the full cavitation model, indicating that different rotating speeds and distribution plate structure would influence cavitation phenomenon. Sun *et al.* (2018) conducted a simulation on the cavitation inside the axial piston water pump, the relationship was established between cavitation degree and the size of the plunger cavity and the waist hole of the cylinder body, it was found that the reasonable design of waist hole size significantly inhibited the cavitation. Tsukiji *et al.* (2015) performed a visual analysis of the cavitation flow inside the axial piston pump, cavitation was observed near the v-shaped groove of the distribution plate with a high-speed camera, they analyzed the cavitation simulation and test results under different operating speeds and various load pressures, and it was found that the two had good consistency. Saxena *et al.* (2008) built a three-dimensional numerical model for fluid flow and cavitation analysis of axial piston pump by Fluent. They found that the end of the distribution port on the distribution plate was prone to high-speed jet flow, they studied its influence on cavitation initiation. Christian *et al.* (2014), ignoring the leakage of the flow field, simulated the fluid domain of the axial piston pump and studied the cavitation at different speeds and angles. Kumar *et al.* (2013) analyzed axial piston pump by simulation, considering the oil film between piston and cylinder clearance condition. They studied the influence of column inserting grooves on cavitation effect, which observed that appropriately increasing the number of grooves and reasonable decoration can inhibit the generation of cavitation; the study also found that the pump cavitation effect has a tendency to increase as the work speed increases. The above research has important significance to the study of cavitation of the rotating-sleeve distribution system.

In terms of the research on RFDS structure, Xu *et al.* (2015) established the kinematic models of three different CAM groove profiles and then analyzed the influence of profiles on the kinematic characteristics of the system. In order to improve the stability of RFDS, Zhang *et al.* (2018) and Jiang *et al.* (2019) optimized the effects of various vibration absorber slots on the flow field characteristics. However, the influence

of RFDS on cavitation has not been investigated. The cavitation model of the system was initially introduced by Zhang *et al.* (2017a, 2017b), who analyzed the influence of cavitation on the water system.

In this study, hydraulic oil was selected as the working medium under constant structure speed and inlet pressure, considering the radial clearance between the rotating-sleeve and the pump body. A complete cavitation model was established based on the fluid domain simulation model with clearance of swivel sleeve. Experimental research was carried out to deeply evaluate cavitation characteristics under various rotating speeds and inlet pressures, as well as the influence of different CAM groove profile structure on cavitation phenomenon of RFDS. In other words, according to the structural characteristics and working form of RFDS, a cavitation simulation model was established to simulate the cavitation characteristics. The cavitation performance of different structures under multiple working conditions was compared and analyzed, and the simulation results were verified by monitoring on the test platform.

## 2. CAVITATION MODEL AND EXPERIMENTAL VERIFICATION

2.1 Cavitation Model

The principle of RFDS is shown in Fig. 1. Through the working principle of the direct acting driving rod cylindrical guide CAM mechanism, RFDS drives the one-way rotation of the rotary sleeve with the linear movement of the plunger. Meanwhile, the distribution port on the rotary sleeve connects with the inlet and outlet oil cavities, respectively, to realize the distribution function (Zhang *et al.* 2015). It is found that the oil film gap between the casing and the pump chamber exhibits significant influence on the operation. The fluid domain model with oil film gap is designed, and Fluent is employed for simulation analysis on the internal flow field of the system. The fluid domain model is shown in Fig. 2.
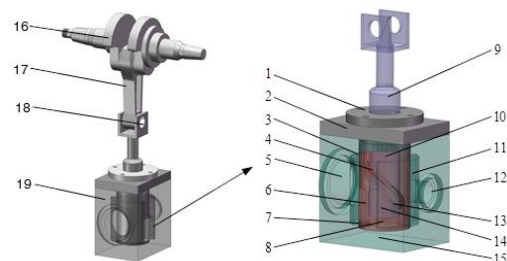
1-guide bush; 2-blind flange; 3-loading chamber; 4-CAM groove; 5-inlet; 6-distribution port; 7-damping groove; 8-pump chamber; 9-plunger; 10-sleeve; 11-collecting chamber; 12-outlet; 13-backing pin; 14-spring; 15-pump body; 16-crankshaft; 17-connecting rod; 18-drive pin; 19-RFDS

Fig. 1. Principle diagram of RFDS.
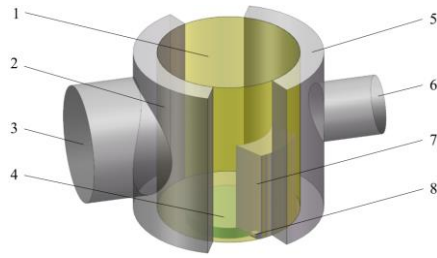
1-clearance of swivel sleeve; 2-loading chamber; 3-inlet; 4-pump chamber; 5-collecting chamber; 6-outlet; 7-valve port; 8-damping groove

Fig. 2. Fluid domain model of a rotating sleeve distribution system.

The hydraulic oil dissolves about 40 ppm of air at room temperature and pressure. When the hydraulic oil flows through distribution system, air will precipitate out and merge into large bubbles if pressure is lower than the air separation pressure of the oil, resulting in cavitation. If the pressure is reduced to the saturated vapor pressure, oil will be evaporated into vapor and the cavitation will intensify. When the mixture of oil and gas flows through the high-pressure position, part of the oil vapor condenses into the oil, and part of the air is dissolved into the oil. The process is accompanied by bubble compression and even collapse, resulting in cavitation corrosion. Cavitation is a difficult barrier in the study of hydraulic system. The commonly used cavitation models are derived from the cavity dynamics equation (Rayleigh-Plesset).

Plesset (1949) took into account the influence of surface tension, steam pressure and liquid viscosity, and improved the Rayleigh equation to form the classic Rayleiy-Plesset equation. A spherical vacuole in an unbounded liquid, where permanent gas and liquid vapor are uniformly distributed inside the bubble, homogeneous liquid is outside the bubble. The basic equation of cavitation dynamics is expressed as follow:

$$RR + \frac{3}{2}\dot{R}^2 = \frac{1}{\rho}\left[p_g + p_v + p_\infty - \frac{2\sigma}{R} - \frac{4\mu\dot{R}}{R}\right], \quad (1)$$

Where R is the surface radius of the bulb; p_g is the pressure in the bubble; p_v denotes the partial pressure of the vapor; σ is the surface tension coefficient of the liquid; μ represents the dynamic viscosity of liquid; p_∞ is the pressure as the radius of the bulb approaches infinity.

The Singhal cavitation model takes the influence of turbulence pressure fluctuation, bubble movement, liquid surface tension and non-condensate gas on the gas phase change into account, the cavitation influence factors considered are more comprehensive. Therefore, the Singhal cavitation model is selected for cavitation simulation of RFDS. Ignoring the influences of second-order terms, liquid viscosity and surface tension on the growth of spherical bubbles, the basic equation of cavitation dynamics can be simplified as:

$$\frac{dR}{dt} = \dot{R} = \sqrt{\frac{2}{3}\frac{p_b - p_c}{\rho}}, \quad (2)$$

Where p_b is the bubble surface pressure; p_c denotes the local far-field pressure.

Since the working medium is a mixture of liquid, vapor and permanent gas, the mixture density can be described as follow:

$$\frac{1}{\rho_m} = \frac{f_v}{\rho_v} + \frac{f_g}{\rho_g} + \frac{1 - f_v - f_g}{\rho_l}, \quad (3)$$

Where ρ_g is the permanent gas density; f_g is the permanent gas mass fraction.

Permanent gas and liquid volume fractions can be expressed as:

$$\alpha_g = f_g \frac{\rho_m}{\rho_g}, \quad (4)$$

$$\alpha_l = 1 - \alpha_v - \alpha_g, \quad (5)$$

The final form of evaporation rate and condensation rate of gas-liquid mass transfer is:

$$s_e = C_e \frac{\sqrt{k}}{\sigma}\rho_l\rho_v\left(1 - f_v - f_g\right)\sqrt{\frac{2}{3}\frac{p'_v - p}{\rho_l}}, \quad (6)$$

$$s_c = C_c \frac{\sqrt{k}}{\sigma}\rho_l\rho_l f_v\sqrt{\frac{2}{3}\frac{p - p'_v}{\rho_l}}, \quad (7)$$

Where ρ_v is the gas phase density, ρ_v=0.4769kg·m^{-3}; ρ_l represents the liquid phase density, ρ_l=865kg·m^{-3}; f_g is the permanent gas mass fraction, f_g=40ppm; f_v is steam mass fraction, f_v=0; p is liquid pressure; p'_v is the saturated vapor pressure, p'_v=400Pa; σ denotes the surface tension coefficient of the liquid, σ = 0.03 N·m^{-1}; Recommended empirical coefficient is C_e=0.02, C_c=0.01.
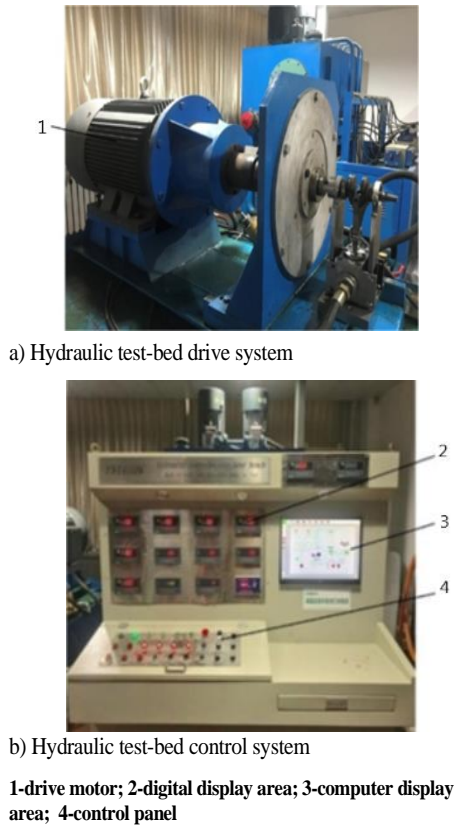
The UFD in Fluent was employed to simulate the fluid field motion and the RNG k-ε turbulence model, First-order upwind discrete processing method, SIMPLE pressure-velocity coupling algorithm was applied to carry out the iterative calculation. The cavitation characteristics of RFDS were discussed and the simulation data was obtained (Zhang *et al.* 2016).
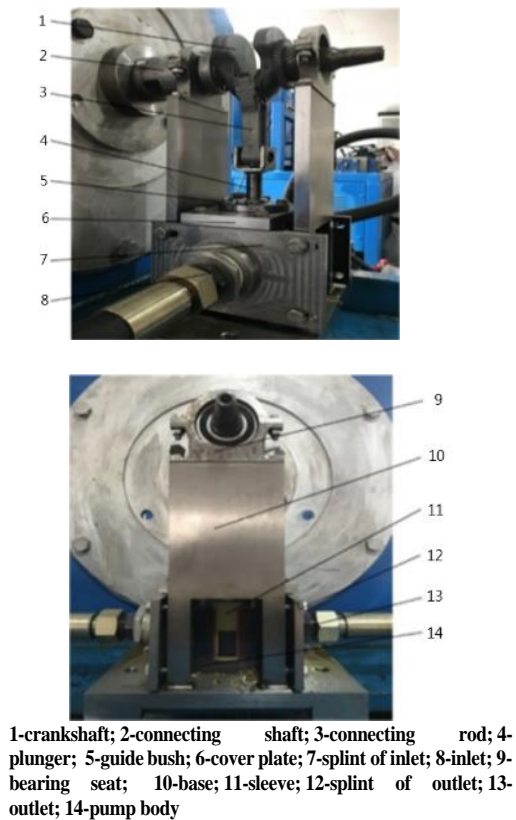
2.2 Experimental Verification

The simulation results of the above section are verified by experiments. The examination was carried out on the YST380W hydraulic integrated test bed shown in Fig. 3. The overall structure of RFDS was designed, processed and assembled on the test bed, as shown in Fig .4. The volumetric efficiency was monitored by the hydraulic integrated test bed and the data can be obtained from the display area.

2.2.1 Speed experiment

The inlet pressure was set as 0.1MPa and the outlet pressure was set as 10MPa, then the volumetric efficiency of the system was simulated and examined under various rotating speeds. The

a) Hydraulic test-bed drive system

b) Hydraulic test-bed control system

1-drive motor; 2-digital display area; 3-computer display area; 4-control panel

Fig. 3. Hydraulic test platform.

1-crankshaft; 2-connecting shaft; 3-connecting rod; 4-plunger; 5-guide bush; 6-cover plate; 7-splint of inlet; 8-inlet; 9-bearing seat; 10-base; 11-sleeve; 12-splint of outlet; 13-outlet; 14-pump body

Fig. 4. Physical prototype of rotating sleeve distribution system.

comparison between the test and simulation data of volume efficiency is shown in Fig. 5, the trend obtained from the test is consistent with the simulation. The experimental data are slightly lower than the simulation results due to the machining error and friction, as the machining error could increase the fit clearance resulting in leakage, and friction causes a reduction in effective power, thus declining volume efficiency. The volumetric efficiency of both the test and the simulation reached its maximum at 500r/min with an error of about 2%.
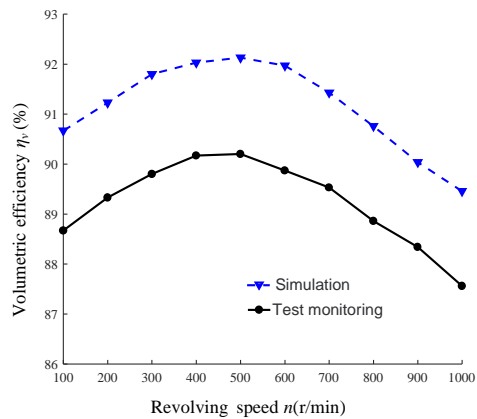
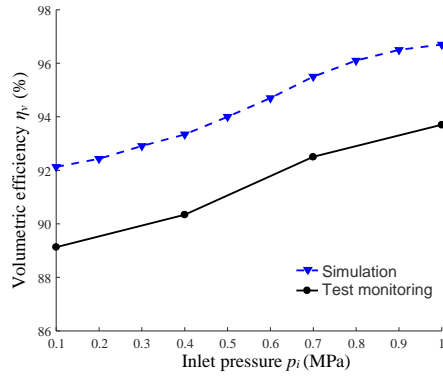**Fig. 5. Volumetric efficiency at different speeds.**

2.2.2 Inlet pressure experiment

The revolving speed was set at 500r/min, and outlet pressure was set at 10MPa. Then, the volumetric efficiency of the system was simulated and experimented by varying the inlet pressure. In the experiment, the inlet pressure was gradually increased with an interval of 0.1MPa. The comparison between experiment and simulation data under various inlet pressures is shown in Fig. 6. The variation trend of the experimental volume efficiency with the inlet pressure is basically consistent with the simulation results. The experimental value is lower than the simulation value, and the maximum error is 3.2% for the influence of machining error and friction, as the machining error could increase the fit clearance resulting in leakage and volume efficiency decline, and friction causes a reduction in effective power. In addition, the current cavitation model is only applicable to the simulation study of cavitation in the distribution system to a certain extent, without considering the dissolution and precipitation properties of non-condensate gases in the actual oil (Liu *et al.* 2020).

The cavitation characteristic experiments verified the cavitation model of RFDS, which laid a foundation for further research. Then the simulation analysis of cavitation characteristics has been done. The parameters of cavitation characteristics include maximum gas volume fraction, cavitation proportion and volume efficiency.

3. EFFECT OF REVOLVING SPEED ON CAVITATION

The inlet and outlet pressure were set as 0.1 MPa and 10 MPa, respectively, to simulate and analyze cavitation characteristics of the system under different revolving speeds.

Fig. 6. Volumetric efficiency at different inlet pressures.

The maximum gas volume fraction α is defined as the ratio of the maximum gas volume generated by cavitation at a certain time in a working cycle to the volume of the fluid domain at that time, which is defined as follows:

$$\alpha = \frac{V_{gmax}}{V} \times 100\% , \tag{8}$$

Where V_{gmax} is the maximum instantaneous gas volume, m³; V denotes the total volume of the system, m³. The larger α leads to greater cavitation intensity and system impact. Cavitation mainly occurs in the distribution port and pump chamber. At different rotating speeds, α's variation trend of the two places is shown in Fig. 7.
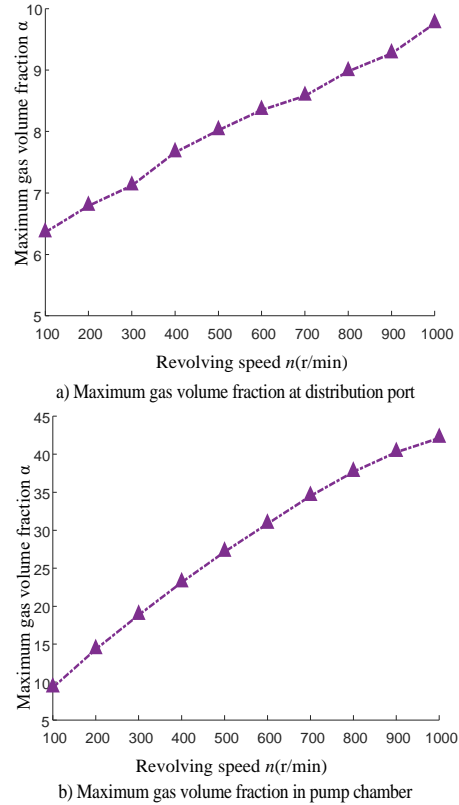
Figure 7 shows that α at both places increases monotonically as the rotating speed increase, the cavitation strength at the distribution port is relatively low. During the simulation process, α is less than 10%. The increased trend in pump chamber is distinct, which can reach more than 40% at a higher speed, which has a great influence on the system.

The relative time of cavitation needs to be investigated, and cavitation time ratio τ is introduced for further quantification. τ is the ratio of cavitation duration to the operating cycle of the system. The larger τ leads to the longer cavitation duration.

$$\tau = \frac{t_c}{T} \times 100\% , \tag{9}$$

Where t_c is cavitation duration of a single working cycle, s; T denotes the working period, s.

The variation trend of τ with the speed is shown in Fig. 8. τ of both places increases continuously as

a) Maximum gas volume fraction at distribution port

b) Maximum gas volume fraction in pump chamber

**Fig. 7. Gas volume fraction at different speeds**

the rotating speed increases. τ at the distribution port is less than 20%; τ in the pump chamber is relatively large within the simulation speed range, reaching more than 20% when the speed is more than 600 r/min, and more than 25% when the speed is more than 800 r/min, indicating that the speed has a significant impact on the cavitation duration.

Volumetric efficiency η_v is an important index of RFDS, which is mainly influenced by oil leakage and cavitation. Cavitation produces gases that block the flow of liquid, reducing the effective volume. η_v is expressed as:

$$\eta_v = \frac{Q_c}{Q_t} \times 100\% , \tag{10}$$

Where, Q_c is the actual output flow, Q_t represents the theoretical output flow, m³/min.

The variation trend of η_v as the function of the speed is shown in Fig. 9. When the rotational speed was at 500 r/min, η_v reached a peak value of 92.13%. The increment of speed will shorten the working cycle, accelerate the flow of oil and reduce the oil leakage in the cycle, leading to the increased η_v; with the further increment of speed, the cavitation degree becomes larger and larger, and the gasification hinders the oil transport, inducing the drop of η_v. Therefore, the speed of 500r/min is the critical point. When the speed is lower than the critical point, the influence of oil leakage on η_v dominates, while the influence of cavitation dominates under the higher speed than the critical point.
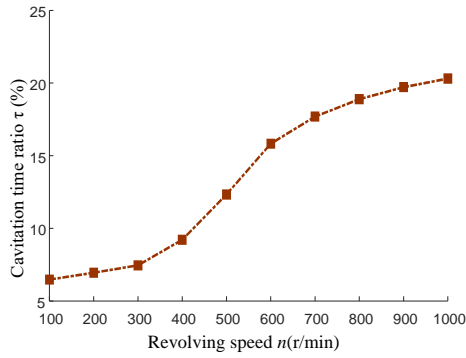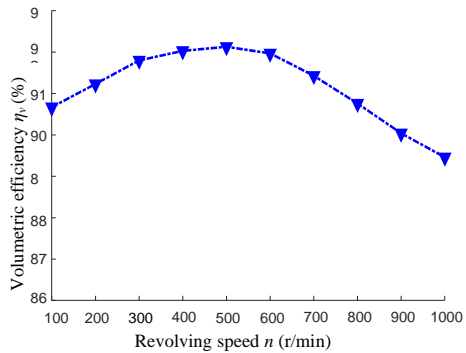
a) Cavitation time ratio at distribution port
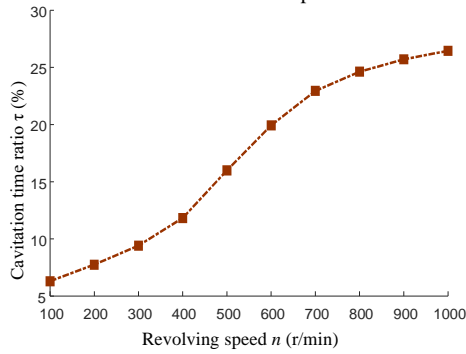
b) Cavitation time ratio in pump chamber
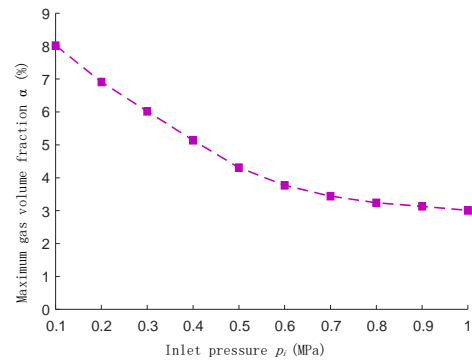
Fig. 8. Cavitation time ratio at different speeds.
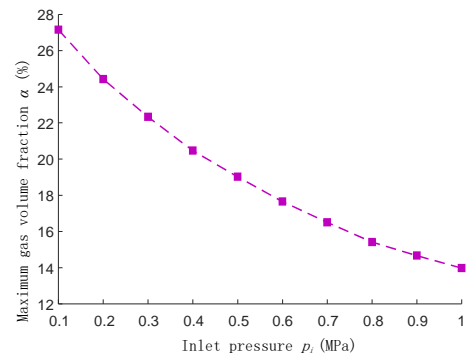

Fig. 9. Volumetric efficiency at different speeds.

a) Maximum gas volume fraction at distribution port

b) Maximum gas volume fraction in pump chamber

Fig. 10. Relationship between maximum gas volume fraction and inlet pressure.

Figure 11 shows the varying trend of τ in the distribution port and the pump chamber with the inlet pressure, τ in both places decreases as the inlet pressure increases. When the inlet pressure is greater than 0.6MPa, τ drops below 10%, indicating that the increased inlet pressure can effectively reduce the cavitation duration.

The change of η_v with inlet pressure is shown in Fig. 12. η_v increases monotonically with the increased inlet pressure, η_v remains above 92% within the simulation pressure range. When inlet pressure is greater than 0.7 MPa, η_v is above 95%. Therefore, increased inlet pressure can reduce cavitation phenomenon.
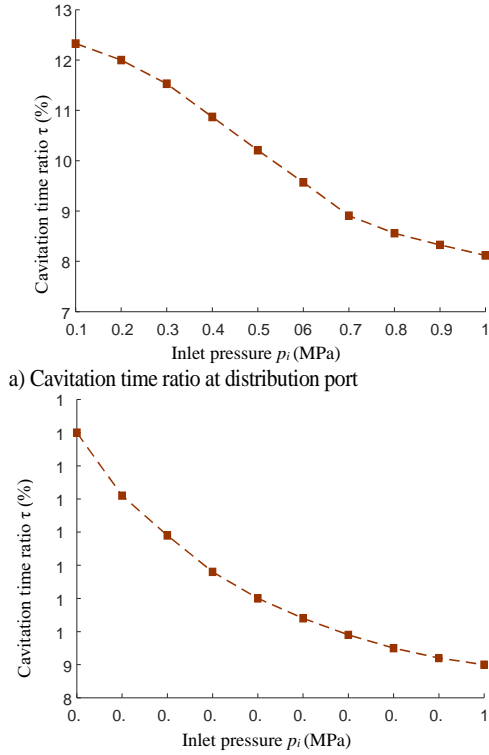
4. INFLUENCE OF INLET PRESSURE ON CAVITATION

Cavitation of RFDS occurs in the initial stage of oil intake, thus the variation of inlet pressure affects the cavitation characteristics of the system. The simulation set the speed at 500r/min and the outlet pressure at 10MPa, then the influence of different inlet pressures on α, τ and η_v of the system was analyzed.

The change of α with inlet pressure is shown in Fig. 10. In both places, α decreases gradually as the inlet pressure enhances. When the inlet pressure is higher than 0.5MPa, α of distribution port decreases to less than 5%. Cavitation strength in the pump chamber varies significantly. α is more than 26% when the inlet pressure is 0.1MPa, while less than 15% when the pressure increases to 0.8MPa.

5. EFFECT OF CAM GROOVE PROFILE ON CAVITATION

5.1 CAM Groove Profile Design

As shown in Fig. 1, the crank connecting rod mechanism drives the plunger to reciprocate. Meanwhile, the sleeve rotates continuously in one direction with the coordination of the internal CAM groove and the transmission pin. The relationship between the axial displacement of the plunger and the crankshaft Angle is as follows:

$$z = r_0(1 - \cos\varphi + \frac{\lambda}{2}\sin^2\varphi) , \qquad (11)$$

Where, z is the axial displacement of the plunger, m; φ is the crankshaft Angle, $\varphi=\omega t$, rad; t is time, s;

a) Cavitation time ratio at distribution port

b) Cavitation time ratio in pump chamber

Fig. 11. Relationship between cavitation time ratio and inlet pressure.

Fig. 12. Relationship between volume efficiency and inlet pressure.

$$\theta_1 = \begin{cases} -\dfrac{\pi}{2}\cos\dfrac{\pi z}{S} + \dfrac{\pi}{2} & (0 \le \varphi \le \pi) \\ \dfrac{\pi}{2}\cos\dfrac{\pi z}{S} + \dfrac{3\pi}{2} & (\pi \le \varphi \le 2\pi) \end{cases}, \quad (13)$$

The relation between the Angle of the linear line rotating sleeve and the crankshaft Angle is as follows:

$$\theta_2 = \begin{cases} \dfrac{\pi z}{S} & (0 \le \varphi \le \pi) \\ 2\pi - \dfrac{\pi z}{S} & (\pi \le \varphi \le 2\pi) \end{cases}, \quad (14)$$

The relation between the corner Angle of the tangent line rotating sleeve and the crankshaft corner is as follows:

$$\theta_3 = \begin{cases} \dfrac{3}{2}\arctan\left(\dfrac{2\sqrt{3}z}{S} - \sqrt{3}\right) + \dfrac{\pi}{2} & (0 \le \varphi \le \pi) \\ \dfrac{3}{2}\arctan\left(\sqrt{3} - \dfrac{2\sqrt{3}z}{S}\right) + \dfrac{3\pi}{2} & (\pi \le \varphi \le 2\pi) \end{cases}$$
$$(15)$$

The relation between the corner Angle of the Spline line rotating sleeve and the crankshaft corner is as follows:

$$\theta_4 = \begin{cases} \dfrac{3\pi z^2}{2S^2} & (\pi \le \varphi \le \dfrac{17}{30}\pi) \\ \pi\left[1 - 3\left(1 - \dfrac{z}{S}\right)^2\right] & (\dfrac{17}{30}\pi \le \varphi \le \pi) \\ \pi\left[1 + 3\left(1 - \dfrac{z}{S}\right)^2\right] & (\pi \le \varphi \le \dfrac{43}{30}\pi) \\ 2\pi - \dfrac{3\pi z^2}{2S^2} & (\dfrac{43}{30}\pi \le \varphi \le 2\pi) \end{cases} \quad (16)$$

Where, z is the function of the piston axial displacement on the crankshaft Angle φ in Eq. (11).

5.2 Cavitation Characteristics Analysis under Calibration Condition

Cavitation simulation study was carried out on the models of four kinds of CAM grooving lines under calibration conditions (inlet pressure is 0.1MPa and outlet pressure is 10MPa at a rotating speed of
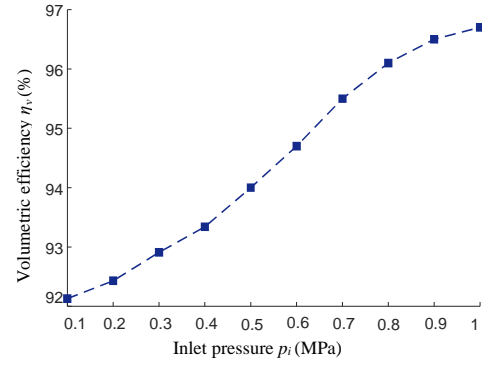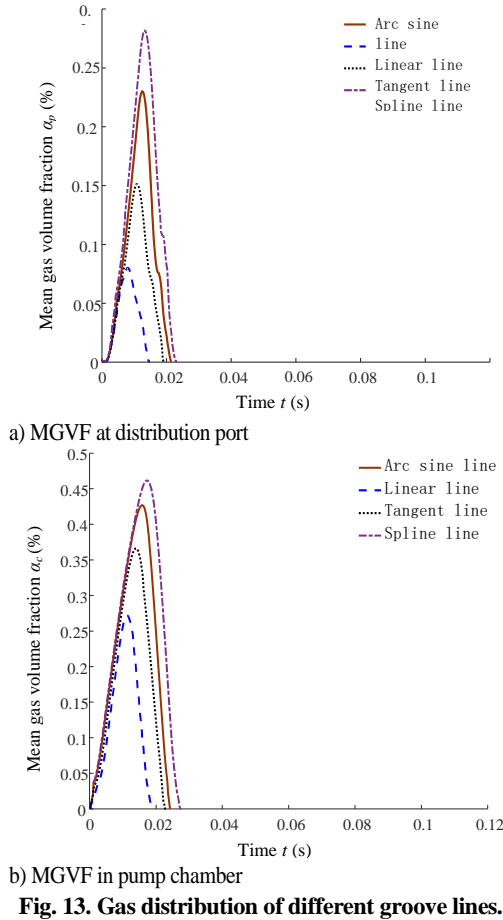
ω is the angular velocity of the crankshaft, $\omega=2\pi n/60$, rad/s; n is the crankshaft speed, r/min; λ is the crank link ratio, $\lambda= r_0/l_0$; r_0 is the crankshaft radius, m; l_0 is the length of the link, m.

The radial depth of the CAM groove is designed to ensure that the sleeve rotates in one direction with the reciprocating motion of the plunger. The radial equation controls the depth variation of the CAM groove, realizing the step at the top and bottom stops. The relationship between depth and turning Angle of the sleeve is expressed as follows:

$$r(\theta) = \begin{cases} \dfrac{d}{2} + h_2 - 3\Delta h\dfrac{\theta^2}{\pi^2} + 2\Delta h\dfrac{\theta^3}{\pi^3} & (0 \le \theta \le \pi) \\ \dfrac{d}{2} + h_2 - 3\Delta h\dfrac{(\theta-\pi)^2}{\pi^2} + 2\Delta h\dfrac{(\theta-\pi)^3}{\pi^3} & (\pi \le \theta \le 2\pi) \end{cases}$$
$$(12)$$

Where, r is the radial depth of the CAM groove, m; d is plunger diameter, m; Δh is CAM groove depth change, $\Delta h=h_2-h_1$, m; h_1 and h_2 denote the respective minimum and maximum depth of the CAM groove, m; θ is the Angle of the sleeve, rad.

In this paper, four kinds of CAM groove structure are designed, which are arcsine profile, linear profile, tangent profile and spline profile. The relationship between the Angle of arcsine line rotating sleeve and the crankshaft Angle is as follows:

a) MGVF at distribution port

b) MGVF in pump chamber

Fig. 13. Gas distribution of different groove lines.

a) Gas volume fraction at distribution port

b) Gas volume fraction in pump chamber

Fig. 14. Relation between gas volume fraction and speed for different profiles.

500r/min). The mean gas distribution of different CAM grooving lines was shown in Fig. 13.

It can be noted from Fig. 13. that the cavitation of spline at the distribution port is the strongest, the arcsine and tangent curves weaken successively, and the linear is the weakest. The variation trend of mean gas volume fraction (MGVF) of each CAM groove profile was same at parts, but the cavitation of the same profile in pump chamber was significantly higher compared with that of distribution port. MGVF of spline profile was up to 46.15%, the cavitation time accounted for 23% of the working cycle. The linear profile with the smallest cavitation had a MGVF of 27.16%, the cavitation time accounted for 16% of the working cycle. The cavitation of linear profile is the weakest, and the duration is the shortest under calibration condition. Linear profile is optimal.

5.3 Cavitation Characteristics Analysis at Different Rotating Speeds

Figure 14 shows the relationship between α of four lines and rotating speeds. At the distribution port, the linear profile had the smallest amplitude increase and α remained below 10% with the increase of rotating speed. The linear profile was less affected by rotating speed. α increment of the spline line was the biggest, which was more than
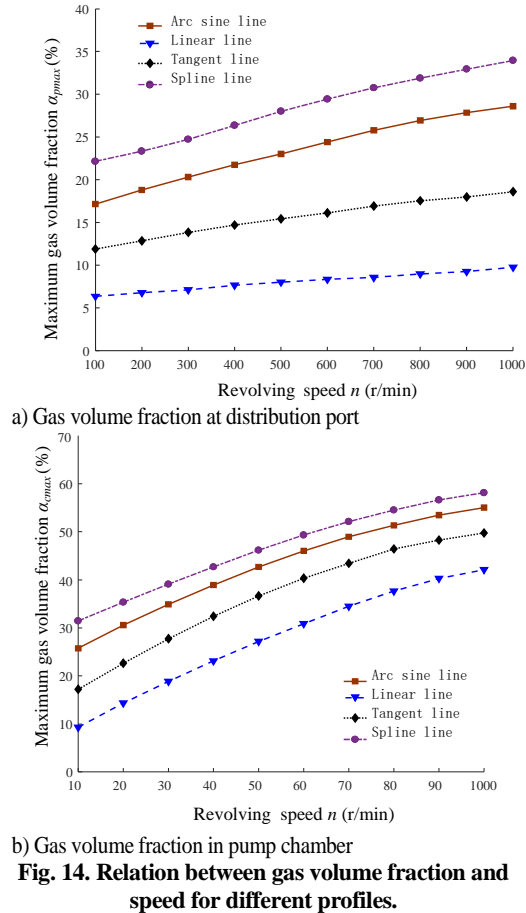
30% at high speed. The cavitation in the pump chamber is stronger than that in the distribution port, α of four CAM groove lines in the high speed are more than 40%, even the spline and arcsine line are more than 50%. Therefore, the linear profile has obvious advantages in a certain speed range.

The variation of τ for the four types with the rotation speed is shown in Fig. 15. In the fluid region of distribution port and pump chamber, τ of linear profile is the minimum at both parts, but τ of the spline profile is the maximum at both parts under the same speed. When the speed is greater than 800r/min, τ of Arcsine, Tangent, Spline lines are more than 20% in distribution port and more than 25% in pump chamber. The cavitation process lasts longer at high speed.

The relationship between the speed and η_v of the four profile lines is shown in Fig. 16. η_v of the linear profile was the highest under the same speed, reaching the maximum value of 92.13% at the speed of 500r/min. η_v of Arcsine, Tangent, Spline lines decrease in order.

5.4 Cavitation Characteristics Analysis under Different Inlet Pressures

The relationship between α of four profiles and the inlet pressure is shown in Fig.17. Decreased trend of spline α became the largest with the increased
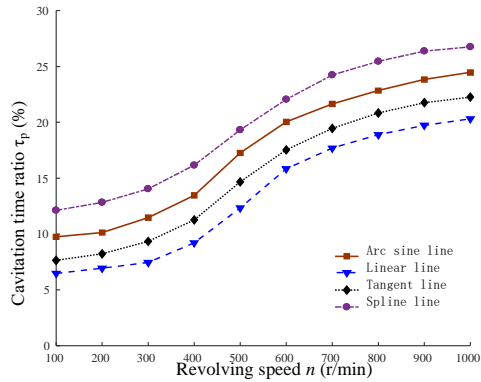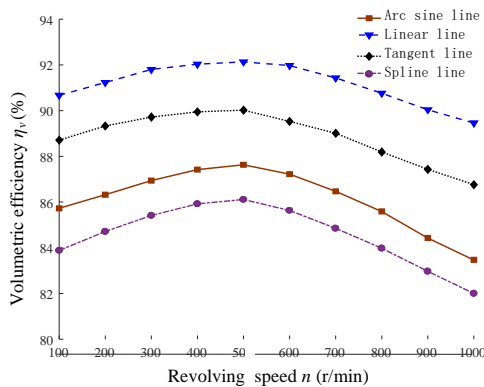
a) Cavitation time ratio at distribution port
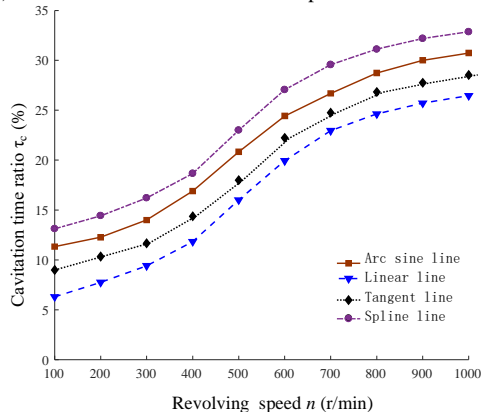
b) Cavitation time ratio in pump chamber

Fig. 15. Relation between cavitation time ratio and speed for different profiles.

Fig. 16. Relation between volumetric efficiency and speed for different profiles.

inlet pressure. The inlet pressure is lower than 0.3MPa at the distribution port, leading to the highest spline profile. When the inlet pressure was higher than 0.3MPa, the spline was lower than the arcsine line, but still higher than others. In the pump chamber, the spline line is lower than the arcsine and tangent line when the inlet pressure is higher than 0.5MPa. In both parts, linear lines have the lowest values.

The relationship between τ of the four profiles and the inlet pressure is shown in Fig. 18. The linear profile exhibits the lowest τ and the shortest cavitation duration. When the inlet pressure is

higher than 0.4MPa, τ becomes lower than the arcsine line. In the pump chamber, τ of spline profile and arctangent profile has a large decline, while tangent profile has a gentle decline for τ. When the inlet pressure is higher than 0.4MPa, τ of tangent profile becomes the highest.

η_v of the four profile under different inlet pressure is shown in Fig.19. When the inlet pressure is higher than 0.5MPa, η_v of Arcsine, Tangent, and Spline lines exceed 90%, η_v increases distinctly as the inlet pressure increases; η_v of linear line grows slower, but η_v is highest under the same inlet pressure, which always stay above 92%, proving the optimal.

The above research shows that the linear profile structure of RFDS is stable with a maintained high volume efficiency, which possesses the best cavitation characteristics in the four kinds of CAM groove profile.
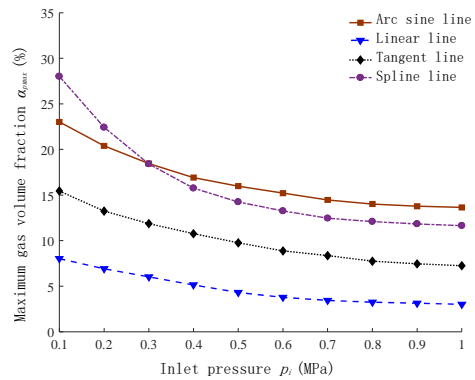
a) Maximum gas volume fraction at distribution port
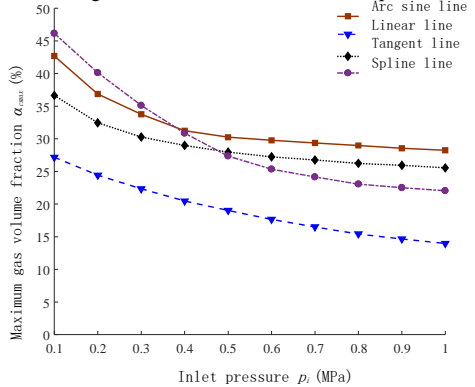
b) Maximum gas volume fraction in pump chamber

Fig. 17. Relation between gas volume fraction and inlet pressure for different profiles.

6. CONCLUSION

1) The cavitation model of RFDS was established and verified by experiments. The experimental volume efficiency was slightly lower than the simulation results, the maximum error was 2% at different rotating speeds, and 3.2% under various inlet pressures.

2) The influence of rotating speed on cavitation characteristics of RFDS was simulated. α increases

a) Cavitation time ratio of distribution port

b) Cavitation time ratio of pump chamber
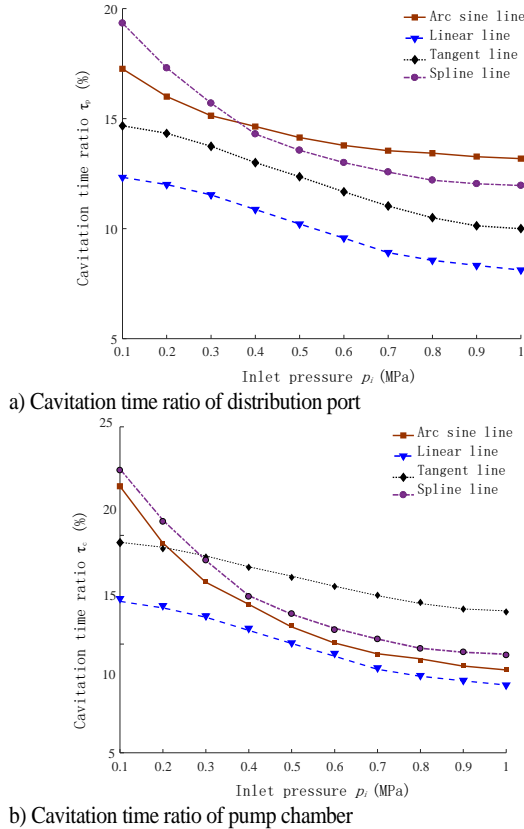
Fig. 18. Relation between cavitation time ratio and inlet pressure for different profiles.
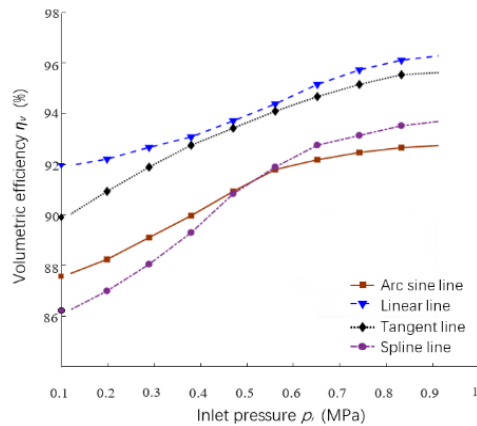
Fig. 19. Relation between volumetric efficiency and inlet pressure for different profiles.

monotonically as the rotating speed increases. The increase rate of α at the distribution port is relatively small, which, however, is relatively large in the pump chamber, exceeding 40% at high rotating speed. τ increases with the increased rotating speed, which at the distribution port is less than 20%, and grows faster than the former in the pump chamber. If the speed is greater than 800r/min, τ will reach more than 25%, and the cavitation in the pump chamber lasts longer; η_v increases first and then decreases with the increased rotational speed, η_v reaches a maximum of 92.13% when the rotating speed reaches 500 r/min.

3) The simulation for influence of inlet pressure on cavitation characteristics of RFDS was performed. In both distribution port and pump chamber, α gradually decreases with the increment of inlet pressure. α is always less than 10% at the distribution port. When inlet pressure in the pump chamber is higher than 0.8MPa, α decreases from 26% to less than 15%, and cavitation decreases significantly with the increased inlet pressure. τ decreases with the increment of inlet pressure. When inlet pressure is greater than 0.6MPa, τ in both places falls below 10%. η_v as inlet pressure increases monotonically, maintaining over 92%, η_v can reach above 95% when inlet pressure is greater than 0.7MPa.

4) Four kinds of CAM groove profile are designed, and the influence of profiles on cavitation is analyzed under the calibration condition. α of spline, arcsine and tangent profile weakened successively, while α of the linear profile was the smallest, which maintained the law at different rotating speeds. τ of four profiles increased as the rotational speed increases. τ of the spline profile was the highest with the longer cavitation duration, while τ of the linear profile was the lowest. η_v of all lines increased first and then decreases with the increased rotational speed, linear lines' η_v is highest with maximum value of 92.13%. η_v of tangent, arcsine and spline decrease in order; Under different inlet pressure, α and τ of linear lines exhibit the lowest value with highest η_v all the time, suggesting that the linear line has a good stability and cavitation characteristics.

REFERENCES

Christian, S. and V. Emmanuel (2014). 3D-CFD simulation of an axial piston displacement unit. *Institute for Fluid Power Drives and Controls (IFAS)*, Steinbachstr 53, D-52074 Aachen, Germany.

Gao, D. X. Suo, Q. Cai, S. Wu and Y. Liang (2018). Influence of key structural parameters on cavitation of hydraulic plunger pump. *China Mechanical Engineering* 29(4), 434-440. (In Chinese)

Huang, B., G. Wang, B. Zhang and Z. Yu (2009). Evaluation of the Cavitation Models on the Numerical Simulation of Cloud Cavitating Flows Around a Hydrofoil. *Journal of Beijing Institute of Technology* 29(9), 785-789 (In Chinese).

Jiang, X., H. Zhang, Q. Zhao, Q. Cheng and Y. Zhang (2019). Optimal Structure Design of U-shaped Damping Groove of Rotating-Sleeve

Distributing-flow System. *Mechanical science and technology* 38(01), 23-29 (in Chinese).

Kumar, S. and J. M. Bergada (2013). The effect of piston grooves performance in all axial piston pumps via CFD analysis. *International Journal of Mechanical Sciences* 66(66), 168-179.

Lao, L., H. Zhou and A. Xie (2015). Design of a high speed single piston pump for piston pair and slipper pair oil film measurement. *Proceeding of the 14th Scandinavian International Conference on Fluid Power.* Tampere: SICFP, 2015.

Liu, C., X. Wu, W. Gan and Y. He (2015). Numerical simulation of cavitation flow in piston pump based on full cavitation model. *China Mechanical Engineering* (24), 3341-3347 (In Chinese).

Liu, R., T. Zhang, H. Zhang, Q. Zhao and S. Du (2020). Influence of Inlet Pressure on Cavitation of Rotary Sleeve Distribution System, *Chinese Hydraulics & Pneumatics* 9. 349, 29-34.

Mikalsen R and A. P. Roskilly (2007). A review of free-piston engine history and applications. *Applied Thermal Engineering* 27, 2339-2352.

Murovec, J., L. Curovic and T. Novakovic (2020). Psychoacoustic approach for cavitation detection in centrifugal pumps. *Applied Acoustics* 165, 107323.

Plesset, M. S. (1949). The Dynamics of Cavitation Bubble. *Journal of Applied Mechanics-Transactions of the ASME* (16), 228-231.

Richard, B., R. F. Medvitz, D. A. Kunz, J. W. Boger, A. N. Lindau, L. Yocum and L. Pauley (2002). Performance analysis of cavitating flow in centrifugal pumps using multiphase CFD. *Journal of Fluids Engineering* 124, 377-383.

Saxena, D. (2008). CFD modeling of cavitation in an axial piston Pump. *Purdue University*.

Schnerr, G. H. and J. Sauer (2001). Physical and Numerical Modeling of Unsteady Cavitation Dynamics. *In: Fourth International Conference on Multiphase Flow*, New Orleans, USA.

Singhal, A. K., M. M. Athavale, H. Y. Li and Y. Jiang (2002). Mathematical Basis and Validation of the Full Cavitation Model. ASME Trans. *Fluids Engineering* 124 (3), 617-624.

Sun, Z., M. Xu, S. Xiao and Y. Dai (2018). Study of simulation and influence of plunger cavity cavitation water axial piston pump. *Journal of system simulation* 30(1), 221-227 (In Chinese).

Wylie, E. M. and V. L. Streeter (1978). Fluid Transients. *Ann Arbor: Michigan University Press.*

Xu, W., H. Zhang and P. Shu (2015). Kinematics Research of Rotating-Sleeve Distributing-Flow System for Reciprocating Plunger Pump. *Advances in Engineering Research* 39, 460-463.

Yuan, S., J. Zhou, X. Luo and C. Jing (2015). Dynamic evolution of gas phase during cavitation of axial piston pump and its influence *Journal of military engineering*, 36(03), 559-565 (In Chinese).

Zhang, H., J. Cheng, T. Zhang, W. Xu and P. Shu (2015). Structure and principle of rotating sleeve flow distribution system for reciprocating plunger pump. *Fluid machinery*, 43(8), 48-51 (In Chinese).

Zhang, H.; T. Zhang, H. Zhao, W. Huo and Y. Zhang (2007). Simulation study on working process of single-cylinder axial internal combustion engine. *Fluid Machinery* 35(3), 1-5 (In Chinese).

Zhang, Y. (2004). Fluid mechanics. *Beijing: higher education press* (in Chinese).

Zhang, Y., H. Zhang, J. Yang, Q. Zhao, X. Jiang, Q. Cheng and Q. Hua (2017b). Research on distribution of flow field and simulation of working pulsation based on rotating-sleeve distributing-flow system. *Modelling and Simulation in Engineering*. vol. 2017: 1-9.

Zhang, Y., H. Zhang, Q. Zhao, X. Jiang and Q. Cheng (2017a). Research of Working Pulsation in Closed Angle Based on Rotating-sleeve Distributing-flow System. *International Conference on Green Energy and Sustainable Development*, 020195.

Zhang, Y., H. Zhang, Q. Zhao, X. Jiang and Q. Cheng (2018). Structure and influence of triangular vibration damping groove on flow field of rotating bushing distribution system. *Journal of mechanical science and technology* 37(06), 834-838 (in Chinese).

Zhang, Y., H. Zhang, Q. Zhao, X. Wang, T. Zhang (2016). Simulation study on pump cavity flow field of rotary sleeve distribution system of reciprocating plunger pump. *Hydraulics and pneumatics* (11), 31-35 (in Chinese).

Zhuo, T. C. and Chen J. (2015). Visual analysis of cavitation flow in axial piston pump. *Chinese Hydraulics & Pneumatics* (2), 1-7.

Zwart P. J., A. G. Gerber and T. Belamri (*2004). A Two-Phase Flow Model for Predicting Cavitation Dynamics* In Proceedings of the Fifth International Conference on Multiphase Flow*, Yokohama, Japan.*